Nonlinear analysis of square steel-reinforced concrete-filled steel tubular short columns considering local buckling

Received: 18 May 2023 | Revised: 21 August 2023 | Accepted: 27 September 2023

DOI: 10.1002/suco.202300402

ARTICLE

fib CEB-FIP WILEY

Nonlinear analysis of square steel-reinforced concrete-filled steel tubular short columns considering local buckling

Mizan Ahmed[1] | **Ramy I. Shahin**[2] | **Saad A. Yehia**[2] | **Mohamed Emara**[3,4] | **Vipulkumar Ishvarbhai Patel**[5] | **Qing Quan Liang**[6]

[1]Centre for Infrastructure Monitoring and Protection, School of Civil and Mechanical Engineering, Curtin University, Bentley, Western Australia, Australia

[2]Department of Civil Engineering, Higher Institute of Engineering and Technology, Kafrelsheikh, Egypt

[3]Structural Engineering Department, Faculty of Engineering, Zagazig University, Zagazig, Egypt

[4]Department of Civil Engineering, Delta Higher Institute for Engineering and Technology, Talkha, Egypt

[5]School of Computing, Engineering and Mathematical Sciences, La Trobe University, Bendigo, Victoria, Australia

[6]College of Sport, Health, and Engineering, Victoria University, Melbourne, Victoria, Australia

Correspondence
Qing Quan Liang, College of Sport, Health, and Engineering, Victoria University, PO Box 14428, Melbourne VIC 8001, Australia.
Email: qing.liang@vu.edu.au

Abstract

This paper presents a fiber element analysis model that simulates the structural responses of square steel-reinforced concrete-filled steel tubular (SRCFST) short columns under concentric compression including local buckling effects. The method of effective widths is utilized to model the gradual postlocal buckling of the steel tube walls of a SRCFST column loaded axially to failure. A new confinement model is developed for the concrete based on test results, considering the confinement induced by the embedded steel section. This confinement model is incorporated into the fiber model, and its accuracy is verified by experimental results. The accuracy of various confinement models proposed for concrete-filled steel tubular (CFST) square columns in predicting the performance of SRCFST columns is evaluated. A parametric study is performed to investigate the performance of SRCFST columns with various parameters. The applicability of the design formulas specified in current standards for CFST columns to the design of SRCFST columns is examined. A formula is proposed to predict the strength of SRCFST short columns. The developed inelastic simulation model, confinement model, and design formula are found to yield performance predictions of SRCFST columns with good accuracy.

KEYWORDS

concrete confinement, fiber element modeling, local buckling. Nonlinear analysis, steel-reinforced concrete-filled steel tubes

1 | INTRODUCTION

Steel-reinforced concrete (SRC) columns are utilized as primary load-carrying members in tall structures and bridge piers because they can withstand significant loads.[1] In a SRC column, the steel section is encased by concrete, thus providing resistance to corrosion in an acidic environment. Despite their numerous benefits, previous studies have indicated that high-strength SRC columns exhibit poor ductility. This is because the high-strength concrete employed in constructing these columns has brittle nature.[1–3] In addition, the construction process of high-strength SRC columns and beam-column connections, which requires the use of formwork, is time-consuming and challenging.[4] Moreover, the formwork must be meticulously constructed and maintained to ensure that the concrete is properly placed and cured, which significantly increases construction costs.

Another type of filled composite column is the concrete-filled steel tubular (CFST) column. The CFST column has higher strength and ductility than the equivalent concrete column due to the concrete confinement provided by the steel tube. In the construction of CFST columns, the steel tube acts as permanent formwork. By eliminating the need for additional formwork, CFST columns can be constructed more efficiently and cost-effectively compared to other types of composite columns. The CFST columns can have various cross-sectional shapes, such as circular, square, or polygonal. It has been found that the circular section offers the most effective confinement to the concrete, while the square or rectangular shape is easier to connect to the adjacent beams.[5]

Zhu et al.[6] studied the behavior of square steel-reinforced concrete-filled steel tubular (SRCFST) column, which combines the structural and construction advantages of both CFST and SRC columns. A SRCFST column consists of an outer square steel box, an internal steel H section or double H section, as illustrated in Figure 1. By offering extra reinforcement and confinement, this design improves the ductility and strength performance of the column.

The study by Zhu et al.[6] involved testing short square SRCFST columns with high-strength concrete under axial compression. The studied parameters were the ratio of width-to-thickness (B/t) of the outer steel box, slenderness ratio, concrete strength, and the reinforcement ratio $(\rho_s)$of the embedded steel section. The primary failure modes of the columns were identified as local buckling developed in the outer tube and the crushing of the internal concrete. The experiments exhibited that the ultimate strength of the columns improved with an increase in the

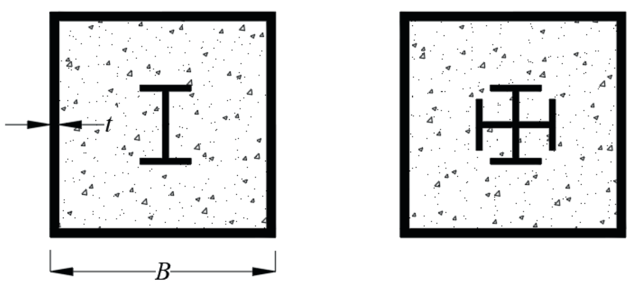

FIGURE 1 Cross-sections of steel-reinforced concrete-filled steel tubular columns. (a) H shape. (b) Double H shape.

concrete strength and ρ_s ratio. Wang et al.[7] conducted a numerical study utilizing a finite element (FE) model to determine the responses of SRCFST columns loaded eccentrically. Their findings revealed an inverse relationship between the loading eccentricity or slenderness ratio and the strength of the column. Ding et al.[4] presented a FE model for SRCFST columns where the behavior of concrete was simulated by the material model of concrete suggested for CFST columns. However, neither Wang et al.[7] nor Ding et al.[4] included the effect of localized instability of the outer steel box in their modeling. More recently, Wang et al.[8] undertook experiments on high-strength SRCFST columns to explore the effects of the ρ_s ratio, yield strength, and thickness of the square box on the behavior of SRCFST columns. It was concluded that using thicker steel tube and higher ρ_s ratio improved the capacity of SRCFST columns.

The literature review shows that only limited research works on SRCFST columns have been undertaken. In addition, existing numerical models for SRCFST columns do not consider the confinement induced by the embedded steel section and the unique local buckling of the outer tube. To address these limitations, a new confinement model is proposed for concrete confined by the steel box and internal steel section and incorporated into the fiber analysis model of SRCFST columns. The proposed computational model accounting for the interaction local buckling of steel tube walls is validated by experimental results. A parametric study is conducted to explore the effects of key parameters on the structural behavior of SRCFST columns. Finally, the results are used to propose a design model for computing the ultimate strength of these columns.

2 | NONLINEAR ANALYSIS USING FIBER DISCRETIZATION

2.1 | Fiber analysis

A model of fiber elements is formulated for the inelastic analysis of axially loaded SRCFST short columns. The column cross-section is meshed with fine fiber elements using a meshing technique developed by Persson and Strang,[9] as presented in Figure 2. The fibers of concrete and steel are given appropriate material properties to characterize their behavior. A perfect longitudinal bond is considered between the concrete and steel fibers to ensure that both materials experience the same axial strain. To predict the axial load-strain response, a step-by-step incremental analysis is proposed and described herein. The axial strain is incrementally increased by a small value, such as 0.0001, and the corresponding axial

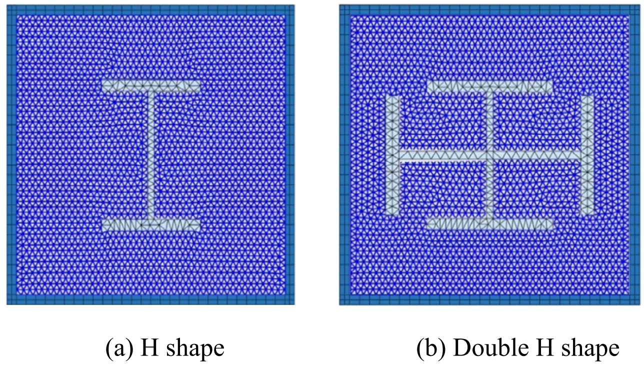

FIGURE 2 Fiber element discretization of steel-reinforced concrete-filled steel tubular column sections. (a) H shape. (b) Double H shape.

stress in each fiber is calculated by using the stress–strain laws. The axial force in each fiber is obtained by multiplying its stress by its cross-sectional area. The axial force in all the fibers is then summed to calculate the applied axial load at that specific axial strain. The numerical analysis continues until the predefined maximum strain (ε_{cu}) is exceeded or the axial load drops below $0.2P_{ult}$. The axial strain-load curve is plotted.

The axial load (P) of the SRCFST column is determined using Equation (1).

$$P=\sum_{i=1}^{ns}\sigma_{s,i}A_{s,i}+\sum_{j=1}^{nc}\sigma_{c,j}A_{c,j} \tag{1}$$

The ductility index of a SRCFST column[10–12] is calculated by

$$PI_{sd}=\frac{\varepsilon_{0.90}}{\varepsilon_y} \tag{2}$$

2.2 | Stress–strain laws for steels

The stress–strain responses of structural steel are illustrated in Figure 3, taking into account the effect of biaxial stresses on the steel box of the SRCFST column owing to the confinement and residual stresses locked in the steel sections. It is assumed that these effects reduce the steel yield stress by 10%.[5,13] The typical yield plateau observed for the mild structural steel is simulated using the tri-linear stress–strain diagram.[14] For the cold-formed steel, the stress–strain curve is curved and for the high-strength steel, the curved part of the cold-formed steel is replaced with a straight line.[14] The curved portion of the curve is predicted by utilizing the equation suggested by Liang,[14] which is expressed as:

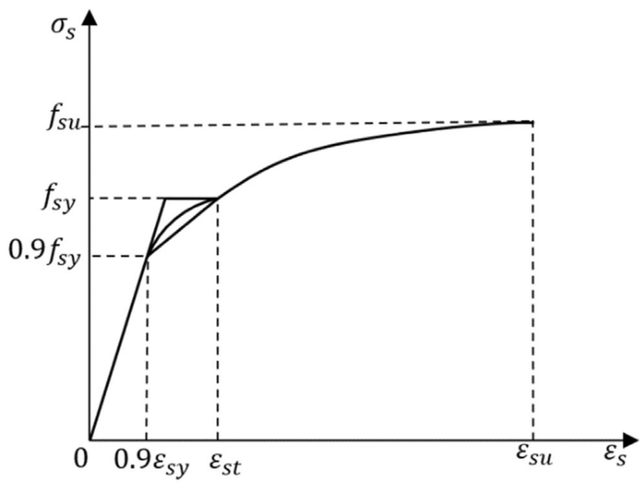

FIGURE 3 Stress–strain behavior of steel material.

$$\frac{\sigma_s}{f_{sy}}=\left(\frac{\varepsilon_s-0.9\varepsilon_{sy}}{\varepsilon_{st}-0.9\varepsilon_{sy}}\right)^{\frac{1}{45}}\left(0.9\varepsilon_{sy}<\varepsilon_s\le\varepsilon_{st}\right) \tag{3}$$

The expressions proposed by Mander[15] are used to compute the stresses of steel fibers beyond the hardening strain ε_{st} until the maximum strain ε_{su}, which is specified as 0.2.

2.3 | Modeling of local buckling of square steel box

Earlier investigations indicate that the failure of square SRCFST columns was caused by the local buckling of the external tube.[6–8] It should be noted that ignoring the influence of localized buckling in the numerical analysis of SRCFST columns results in an overestimation of their structural performance. To address this issue, this study uses expressions proposed by Liang et al.[16] for the steel tube walls of a rectangular CFST column to simulate the local and post-local buckling of the steel tube in SRCFST columns. During numerical calculations, the steel fiber stress is continuously monitored to identify any potential local buckling in comparison to the initial local buckling stress. Liang et al.[16] proposed formula for calculating the initial local buckling stress of the steel tube walls in a rectangular CFST column subjected to uniform compressive stresses as follows:

$$\frac{\sigma_{cr}}{f_{syo}}=0.5507+0.005132\left(\frac{b}{t}\right)-9.869\times10^{-5}\left(\frac{b}{t}\right)^2+1.198\times10^{-7}\left(\frac{b}{t}\right)^3 \tag{4}$$

in which and t is the thickness of the steel tube, f_{syo} and $\sigma_{cr}$are the yield stress and initial local buckling stress of the steel tube wall, respectively.

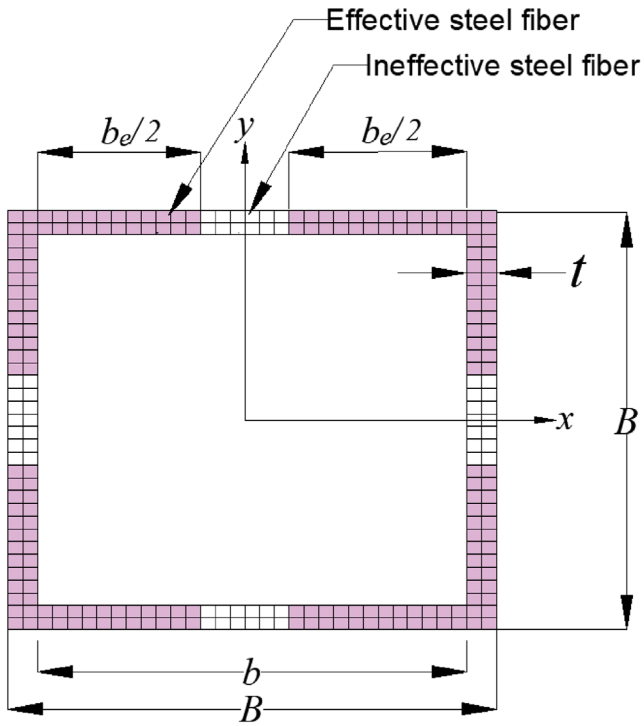

FIGURE 4 Effective width of the square tube of steel-reinforced concrete-filled steel tubular column under axial loading.

The stress redistribution method is used to simulate the progressive postlocal buckling behavior of steel plates under the increasing load. In the simulation, the stresses are redistributed from the heavily buckled region to the unloaded edge strips of the steel tube. The effective width concept is utilized to simulate the progressive postlocal buckling of the outer tube as shown in Figure 4. Liang et al.[16] developed an expression for the effective width of the steel tube walls, which is written as

$$\frac{b_e}{b} = 0.5554 + 0.02038\left(\frac{b}{t}\right) - 3.944\times10^{-4}\left(\frac{b}{t}\right)^2 + 1.921\times10^{-6}\left(\frac{b}{t}\right)^3 \tag{5}$$

in which b and b_e are the clear width and the effective width of the steel tube wall, respectively.

The ineffective width b_{ne} can be calculated by linear interpolation depending on the stress level of the steel fibers using the following expression:

$$b_{ne} = b_{ne,max}\left(\frac{\sigma_s - \sigma_{cr}}{f_{syo} - \sigma_{cr}}\right) \tag{6}$$

The maximum ineffective width $b_{ne,max}$ of the steel tube wall is determined as

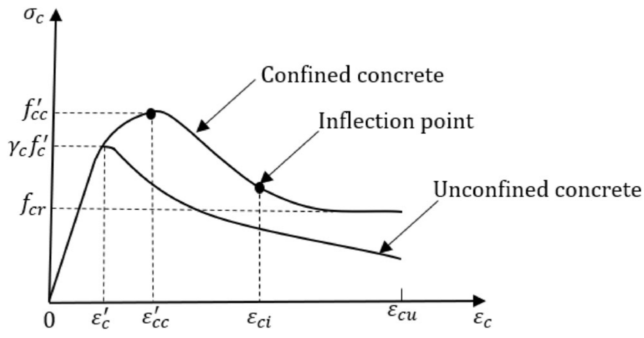

FIGURE 5 Stress–strain constitutive curves for concrete with and without confinement.

$$b_{ne,max} = b - b_e \tag{7}$$

In the numerical modeling, the stresses of the steel fibers are first calculated by using the stress–strain relationships of steel and checked for possible local buckling. When the b/t ratio of the steel tube wall is >30 and steel stress is greater than the critical local buckling stress, the ineffective width of the steel tube is computed. The stresses of fiber in the ineffective region are taken as zero until the maximum $b_{ne,max}$ is attained.

2.4 | Concrete material modeling

The concrete model depicted in Figure 5 is utilized in this study to determine the ascending portion of the curve expressed as.

$$\sigma_c = \frac{f'_{cc}(\varepsilon_c/\varepsilon'_{cc})\lambda}{(\varepsilon_c/\varepsilon'_{cc})^{\lambda} + \lambda - 1} \quad \text{for } 0 \le \varepsilon_c \le \varepsilon'_{cc} \tag{8}$$

$$\lambda = \frac{E_c\varepsilon'_{cc}}{E_c\varepsilon'_{cc} - f'_{cc}} \tag{9}$$

Equation (8) was suggested by Mander et al.[17] The concrete modulus of elasticity (E_c) is computed using Equation (10).[18]

$$E_c = 4400\sqrt{\gamma_c f'_c}\ (\text{MPa}) \tag{10}$$

In Equation (10), γ_c is the reduction factor, which considers the column size effect, was suggested by Liang[14] as $\gamma_c = 1.85 D_c^{-0.135}$, where D_c is taken as $(B - 2t)$ for the SRCFST column.

Equation (11) is utilized to determine the concrete compressive strength (f'_{cc}) in SRCFST columns.[17]

$$f'_{cc} = \left(1 + \frac{4.1 f_{rp}}{\gamma_c f'_c}\right) \gamma_c f'_c \tag{11}$$

The lateral pressure induced by the confinement factor (ξ) of SRCFST columns is calculated using Equation (12).

$$\xi = \frac{A_{st} f_{sy,T} + A_{ss} f_{sy,S}}{A_c \gamma_c f'_c} \tag{12}$$

Based on the experimental works of Zhu et al.,[6] Wang et al.,[7] and Wang et al.,[8] a new expression for calculating the confining pressure (f_{rp}) is proposed as

$$f_{rp} = 1.2818\xi + 4.8267 \tag{13}$$

To derive Equation (13), the section capacities of steel tube and embedded steel section of the SRCFST column were first subtracted from the ultimate axial load of the column. Equation (7) was then used to evaluate $f_{rp,test}$ for each of the tested columns. Finally, the confinement factor (ξ) of each tested column was plotted against the measured $f_{rp,test}$ and a linear equation was proposed based on the statistical analysis, as demonstrated in Figure 6.

The compressive strain (ε'_{cc}) of confined concrete is estimated by means of employing the expression recommended by Wang et al.[19] as

$$\varepsilon'_{cc} = 2300 + 31.2\left(\gamma_c f'_c\right)^{0.7} + \left[2.32 \times 10^4 - 3.88 \times 10^6 \left(\gamma_c f'_c\right)^{-1.8}\right] \left(\frac{t f_{sy,T}}{B \gamma_c f'_c}\right)^2 \tag{14}$$

The descending part of the curve is determined by

$$\sigma_c = f'_{cc} - \frac{f'_{cc} - f_{cr}}{1 + \left(\frac{\varepsilon_c - \varepsilon'_{cc}}{\varepsilon_{ci} - \varepsilon'_{cc}}\right)^{-2}} \quad \text{for } \varepsilon_c > \varepsilon'_{cc} \tag{15}$$

Equation (15) was proposed by Lim and Ozbakkaloglu[20] where ε_{ci} stands for the strain at the inflection point as presented in Figure 5, equals to 0.01; f_{cr} represents the residual strength of concrete computed as $f_{cr} = \beta_c f'_{cc}$ in which β_c denotes a strength reduction factor ($0.1 \le \beta_c \le 1$). After analyzing the experimental data reported by Zhu et al.[6] and Xiong et al.,[21] β_c is proposed as

$$\beta_c = 0.5114\xi\text{-}0.1572 \tag{16}$$

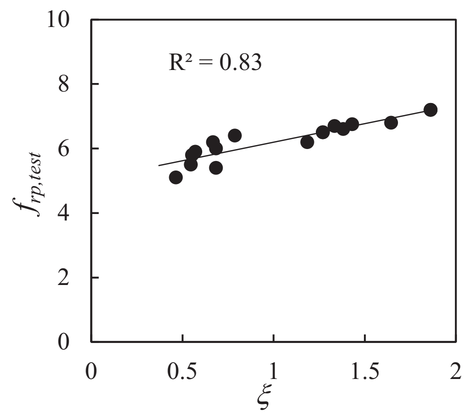

FIGURE 6 Validation of the proposed formula for concrete confinement f_{rp}.

3 | VALIDATIONS OF NUMERICAL MODEL

3.1 | Comparison with experimental results

The predicted ultimate strengths of SRCFST columns by the numerical model are compared with test results in Table 1 to validate its accuracy. It should be noted that the strength of the concrete cube stated in the experiments has been converted to the cylindrical strength by multiplying the cube strength by 0.85.[22] It can be observed from Table 1 that the agreement between experimental data and numerical results is excellent. The average value of the predicted and experimental ultimate strength is 0.99. The computed axial load-strain diagrams of SRCFST columns are compared with experimental data in Figure 7. It appears that the developed numerical model, which incorporates the newly proposed confinement model, accurately computes the experimentally measured axial strain-load relationships of SRCFST columns.

4 | ASSESSMENTS OF EXISTING CONFINEMENT MODELS

This section assesses the reliability of existing confinement models in predicting the structural responses of short SRCFST columns. Table 2 presents the confinement models proposed by Lai and Varma,[13] Hu et al.,[23] Thai et al.,[24] and Tao et al.[25] These confinement models have been implemented in the fiber-based modeling program for SRCST columns. The experimental results and computed ultimate strengths using various confinement models are compared in Table 3. It is shown that these

TABLE 1 Ultimate axial loads of steel-reinforced concrete-filled steel tubular (SRCFST) short columns.

Column	B (mm)	t (mm)	B/t	A_{ss} (mm^2)	$f_{sy,T}$ (MPa)	$f_{sy,S}$ (MPa)	f'_c (MPa)	$P_{u,exp}$ (kN)	$P_{u,num}$ (kN)	$\frac{P_{u,num}}{P_{u,exp}}$	Ref.
S5L10V	195	5.5	35	2866	288	338	41.1	4035	3970	0.98	Zhu et al.[6]
S5L10	195	5.5	35	2866	288	338	41.1	4050	3970	0.98	
S5H10V	195	5.5	35	2866	288	338	60.2	4880	4553	0.93	
S5H10	195	5.5	35	2866	288	338	60.2	4880	4553	0.93	
S4L10	195	4.5	43	2866	289	338	41.1	3930	3963	1.01	
S4H10	195	4.5	43	2866	289	338	60.2	4750	4424	0.93	
S4L10I	195	4.5	43	1433	289	338	41.1	3410	3495	1.02	
S4H14	195	4.5	43	3870	289	327	60.2	4710	4672	0.99	
S5L10I	195	5.5	35	1433	288	338	41.1	3620	3676	1.02	
PY10I-0-3	200	5	40	1350	355	355	41.1	3740	3909	1.05	Wang et al.[7]
STSRC235-3-H	180	3	60	1415	327	288	89.3	3729	3955	1.06	Wang et al.[8]
STSRC235-4-H	180	4	45	1415	327	288	89.3	4239	4210	0.99	
STSRC235-5-H	180	5	36	1415	327	288	89.3	4545	4378	0.96	
STSRC345-3-H	180	3	60	1415	420	288	89.3	4114	4222	1.03	
STSRC345-4-H	180	4	45	1415	420	288	89.3	4231	4466	1.06	
STSRC235-2-DH	180	2	90	2830	327	288	89.3	4153	4124	0.99	
STSRC235-3-DH	180	3	60	2830	327	288	89.3	4553	4315	0.95	
STSRC235-4-DH	180	4	45	2830	327	288	89.3	4577	4492	0.98	
STSRC235-3DH*	180	3	60	725	327	288	89.3	4223	3895	0.92	
Mean										0.99	
Standard deviation (SD)										0.04	
Coefficients of variance (CoV)										0.04	

confinement models mentioned above result in an underestimation of the column ultimate loads. This is because these confinement models ignore the effect of confinement induced by the embedded sections on the core concrete. The confinement models proposed by Lai and Varma,[13] Hu et al.,[23] Thai et al.,[24] and Tao et al.[25] result in an average predicted-to-experimental ultimate strength ratio of 0.84, 0.88, 0.88, and 0.90, respectively. Figure 8 compares the predicted axial load-strain diagrams of SRCFST columns with test results. It appears that there are significant discrepancies between the experiments and predictions when using existing confinement models. However, the proposed concrete confinement model in this study provides better predictions than the existing models, as shown in Table 1 and Figure 8.

5 | BEHAVIOR OF SRCFST COLUMNS

Various parameters that can affect the structural responses of SRCFST columns were examined using this proposed fiber model. A reference column was considered with an external square tube having a 600-mm width and a 10-mm thickness, embedded steel section area of 3757 mm^2, concrete strength of 70 MPa, and an external and embedded steel yield stress of 350 MPa. Five different groups (G1–G5) of SRCFST columns were studied to investigate the effects of the width-to-thickness B/t ratio, steel reinforcement ratio of the embedded steel section, concrete strength, yield strength of the outer steel box, and the yield stress of the embedded steel section. Details of the reference and analyzed columns are provided in Table 4.

5.1 | Influence of B/t ratio

The fiber-based computer model was used to quantify how the width-to-thickness B/t ratio affects the performance of SRCFST columns. The B/t ratio was calculated by altering the thickness of the tube for the same width. Table 4 and Figure 9 demonstrate that the axial capacity of the columns reduces significantly as the B/t

FIGURE 7 Comparison of measured and predicted axial load-strain responses of steel-reinforced concrete-filled steel tubular columns using the proposed confinement model.

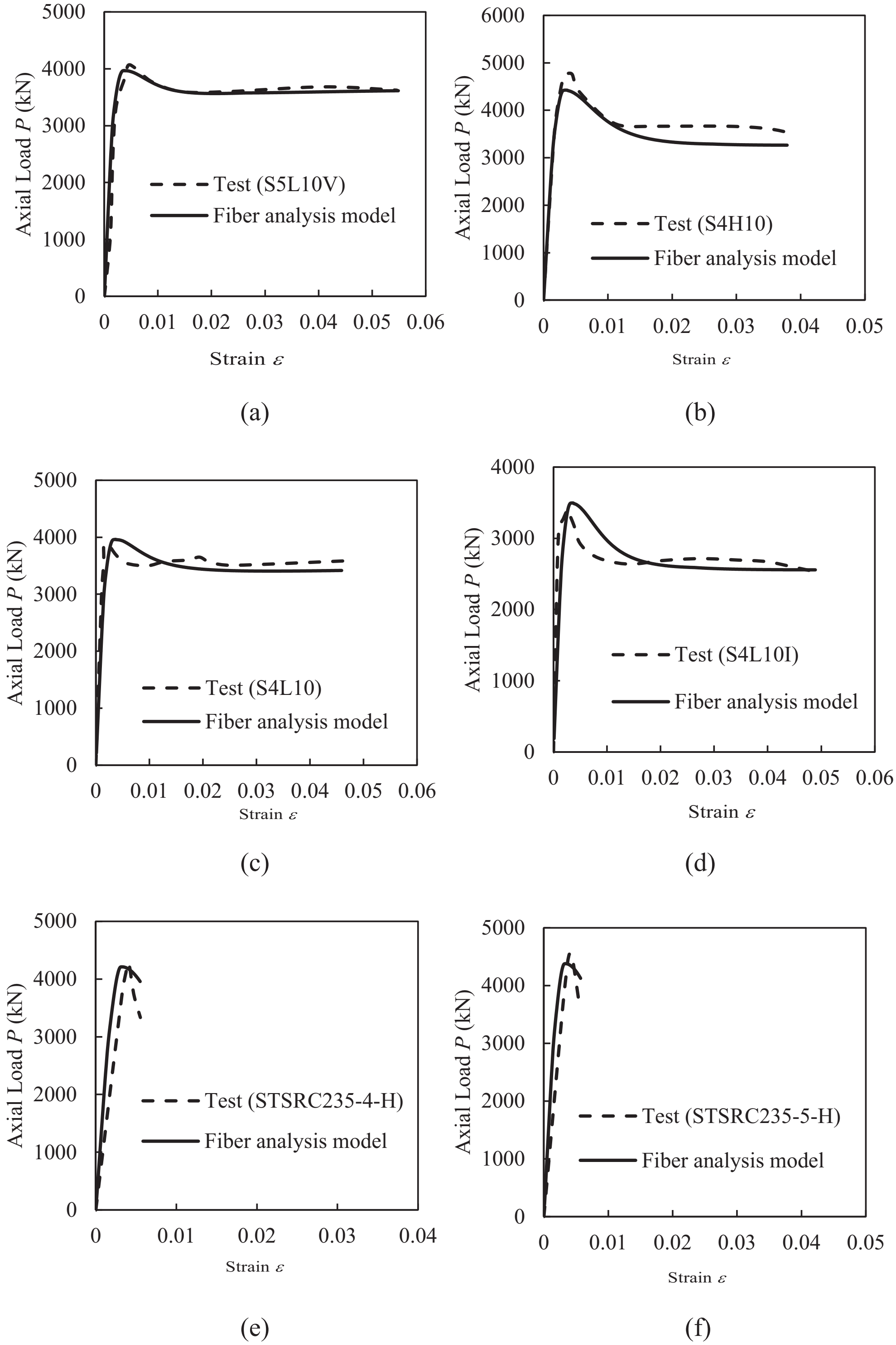

ratio increases. Changing the B/t ratio from 40 to 100 causes a reduction of 17.2% in the ultimate strength of the columns. Moreover, Figure 10 shows that the ductility index decreases with increasing the B/t ratio. If the B/t ratio is increased, the local buckling of the outer tube may take place. Therefore, increasing this ratio leads to a reduction in the ductility and strength of the columns.

5.2 | Influence of embedded steel reinforcement ratio

The influence of the ρ_s ratio of the embedded steel section on the responses of SRCFST columns was assessed by varying the ratio from 1.04% to 2.09%, 3.12%, and 4.18%. As depicted in Figure 11, it is apparent that the ρ_s ratio has a minor effect on the performance of the

TABLE 2 Existing concrete confinement models for concrete-filled steel tubular (CFST) columns.

Confinement model	Formulas for calculating the compressive concrete strength (f'_{cc})	Formulas for calculating (β_c)
Hu et al.[23]	$\frac{f'_{cc}}{f'_c}=1+4.1\left(\frac{f_{rp,1}}{f'_c}\right)$ $\frac{f_{rp,1}}{f_{sy}}=\begin{cases}0.055048-0.001885(B/t) & \text{for } 17\le B/t\le 29.2\\ 0 & \text{for } 29.2<B/t\le 150\end{cases}$	If $17\le B/t\le 70$, $\beta_c=0.000178\ (B/t)^2-0.02492\ (B/t)\ +\ 1.2722$ If $70\ <\ B/t\ \le\ 150$, $\beta_c\ =\ 0.4$
Thai et al.[24]	$\frac{f'_{cc}}{f'_c}=1+3.24\left(\frac{f_{rp,2}}{f'_c}\right)^{0.8}$ $f_{rp,2}=\begin{cases}\frac{\left(195.118+40.611f_{sy}\right)e^{-.01(B/t)}}{988-0.01962f'_c} & \text{for } B/t\le 15\\ \frac{\left(-42,428+236f_{sy}\right)e^{-.04(B/t)}}{7773+\left(f'_c\right)^{1.6}} & \text{for } B/t>15\end{cases}$	$\beta_c=0.1$
Lai and Varma[13]	$\frac{f'_{cc}}{f'_c}=0.8+0.18\left(\frac{B/t}{100}+\frac{f_{sy}/f'_c}{30}\right)\le 1.10$	The postpeak behavior of concrete is similar to the unconfined concrete model
Tao et al.[25]	$\frac{f'_{cc}}{f'_c}=\gamma_c\left[0.845+\frac{f_{sy}^{0.08}}{2\left(f'_c\right)^{0.4}}+\frac{0.35(\xi_c)^{1.06}}{\left(D'/t\right)^{0.3}}\left(\frac{B}{H}\right)\right]$ $\gamma_c=\left(\frac{D_c}{212}\right)^{-0.14}\le 1.05$ $D_c=\sqrt{(B-2t)^2+(H-2t)^2}$ $D'=\sqrt{B^2+H^2}$ $B=H$ for square columns	$\beta_c=0.96\xi^{0.1}+\frac{9.7}{\left(D'/t\right)^{1.5}}+0.09\sqrt{\frac{f_{sy}}{f'_c}\frac{B}{H}}-0.7$ $(0.15\le\beta_c\le 1.0)$

columns, especially on the ductility. However, it is discovered that increasing ρ_s ratio from 1.04% to 4.18% results in a 9.3% increase in the ultimate strength of the columns. Figure 12 illustrates that the ductility index slightly increases from 2.68 to 2.98 when increasing the ρ_s ratio from 1.04% to 4.18%. The additional steel reinforcement enhances the overall strength of the column by providing additional steel area and confinement to the concrete, thus preventing premature failure. The reinforcement also increases the ductility of the column by enabling it to undergo more significant deformation before failing.

5.3 | Influence of concrete strength

The computational simulation was performed to assess the effects of concrete compressive strength on the performance of SRCFST columns. The study involved varying the concrete strength from 30 to 90 MPa. Figure 13 compares the axial load-strain relationships as a function of concrete strength. It is shown that increasing the concrete strength remarkably improves the column's resistance but considerably decreases its ductility due to the brittle behavior of high-strength concrete. It is noted from Figure 14 that the ultimate strength of the columns improves by 61% when changing the concrete strength from 30 to 90 MPa. The column with a concrete strength of 30 MPa has a ductility index of 3.55, while the column with a concrete strength of 90 MPa has a ductility index of 2.49.

5.4 | Effects of yield stress

The response of SRCFST columns was studied by varying the yield strength of the external tube and embedded steel section from 250 to 550 MPa. The diagrams of axial load-strain as presented in Figure 15 reveal that the steel yield stress of the external tube has a greater influence on the performance of SRCFST columns than that of the embedded steel section. This is because the cross-sectional area of the external tube is larger than that of the internal steel section. Changing the yield stress of the steel box from 250 to 550 MPa results in a substantial increase of 20.6% in the ultimate load of the SRCFST column. On the other hand, when the yield stress of the embedded steel section is raised from 250 to 550 MPa, the ultimate load of the SRCFST column increases only 3.3%.

TABLE 3 Ultimate strengths of steel-reinforced concrete-filled steel tubular (SRCFST) columns obtained by different confinement models.

		Hu et al.[23]		Thai et al.[24]		Lai and Varma[13]		Tao et al.[25]	
Specimen	$P_{u,exp}$ (kN)	$P_{u,num1}$ (kN)	$\frac{P_{u,num1}}{P_{u,exp}}$	$P_{u,num2}$ (kN)	$\frac{P_{u,num2}}{P_{u,exp}}$	$P_{u,num3}$ (kN)	$\frac{P_{u,num3}}{P_{u,exp}}$	$P_{u,num4}$ (kN)	$\frac{P_{u,num4}}{P_{u,exp}}$
S5L10V	4035	3335	0.83	3502	0.87	3443	0.85	3694	0.92
S5L10	4050	3335	0.82	3502	0.86	3443	0.85	3694	0.91
S5H10V	4880	3876	0.79	4052	0.83	4035	0.83	4231	0.87
S5H10	4880	3876	0.79	4052	0.83	4035	0.83	4231	0.87
S4L10	3930	3151	0.80	3285	0.84	3264	0.83	3472	0.88
S4H10	4750	3705	0.78	3870	0.81	3870	0.81	4022	0.85
S4L10I	3410	2721	0.80	2861	0.84	2838	0.83	2989	0.88
S4H14	4710	3946	0.84	4106	0.87	4106	0.87	4295	0.91
S5L10I	3620	2904	0.80	3079	0.85	3018	0.83	3207	0.89
PY10I-0-3	3740	3166	0.85	3404	0.91	3292	0.88	3493	0.93
STSRC235-3-H	3729	3477	0.93	3679	0.99	3679	0.99	3669	0.98
STSRC235-4-H	4239	3650	0.86	3844	0.91	3844	0.91	3875	0.91
STSRC235-5-H	4545	3821	0.84	4022	0.88	4006	0.88	4080	0.90
STSRC345-3-H	4114	3674	0.89	3877	0.94	3877	0.94	3893	0.95
STSRC345-4-H	4231	3912	0.92	4141	0.98	4106	0.97	4172	0.99
STSRC235-2-DH	4153	3593	0.87	3794	0.91	3794	0.91	3787	0.91
STSRC235-3-DH	4553	3768	0.83	3961	0.87	3961	0.87	3997	0.88
STSRC235-4-DH	4577	3941	0.86	4125	0.90	4125	0.90	4207	0.92
STSRC235-3DH*	4223	3335	0.79	3542	0.84	3542	0.84	3510	0.83
Mean			0.84		0.88		0.88		0.90
Standard deviation (SD)			0.04		0.05		0.05		0.04
Coefficients of variance (CoV)			0.05		0.06		0.06		0.05

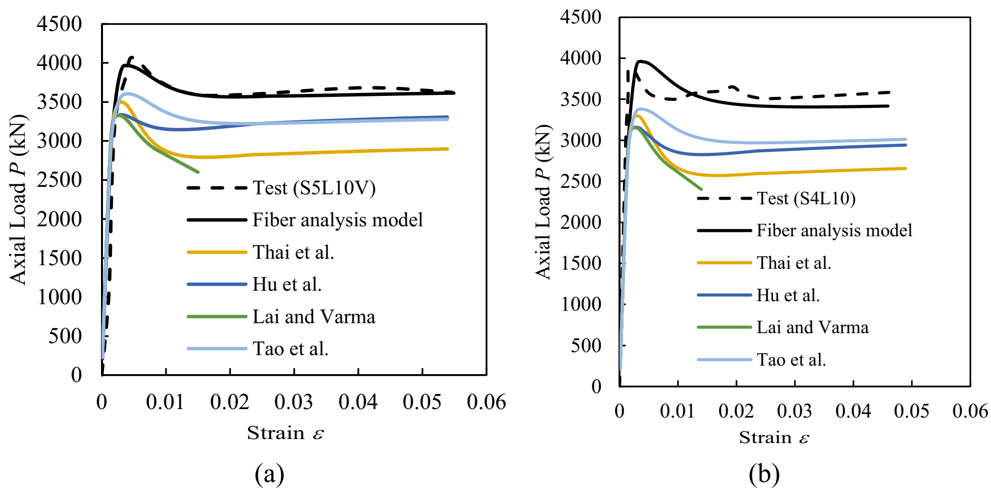

FIGURE 8 Evaluating the accuracy of various concrete confinement models.

5.5 | Influence of concrete confinement

The importance of concrete confinement on the performance of SRCFST columns was studied. For this purpose, the reference column was analyzed by either considering the concrete confinement or ignoring it. The results obtained are presented in Figure 16. It appears that ignoring concrete confinement leads to an

TABLE 4 Material and geometric properties of columns investigated in the parametric study.

Group	Column	B (mm)	t (mm)	B/t	A_{ss} (mm^2)	$f_{sy,T}$ (MPa)	$f_{sy,S}$ (MPa)	f'_c (MPa)	$P_{u,num}$ (kN)
G1	SRCSFT 1	600	15	40	3757	350	350	70	39,293
	SRCSFT 2	600	10	60	3757	350	350	70	35,833
	SRCSFT 3	600	7.5	80	3757	350	350	70	33,888
	SRCSFT 4	600	6	100	3757	350	350	70	32,542
G2	SRCSFT 5	600	10	60	3757	350	350	70	35,833
	SRCSFT 6	600	10	60	7514	350	350	70	36,942
	SRCSFT 7	600	10	60	11,230	350	350	70	38,040
	SRCSFT 8	600	10	60	15,056	350	350	70	39,170
G3	SRCSFT 9	600	10	60	3757	350	350	30	25,645
	SRCSFT 10	600	10	60	3757	350	350	50	30,518
	SRCSFT 11	600	10	60	3757	350	350	70	35,833
	SRCSFT 12	600	10	60	3757	350	350	90	41,301
G4	SRCSFT 13	600	10	60	3757	250	350	70	33,516
	SRCSFT 14	600	10	60	3757	350	350	70	35,833
	SRCSFT 15	600	10	60	3757	450	350	70	38,123
	SRCSFT 16	600	10	60	3757	550	350	70	40,410
G5	SRCSFT 17	600	10	60	3757	350	250	70	35,433
	SRCSFT 18	600	10	60	3757	350	350	70	35,833
	SRCSFT 19	600	10	60	3757	350	450	70	36,227
	SRCSFT 20	600	10	60	3757	350	550	70	36,611

Abbreviation: SRCFST, steel-reinforced concrete-filled steel tubular.

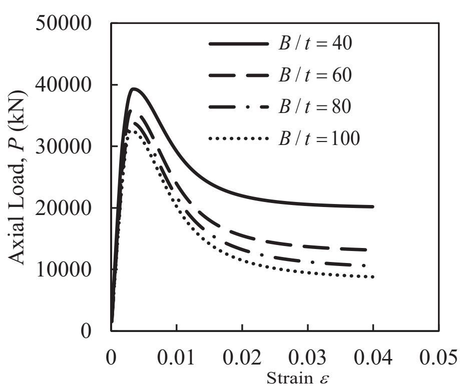

FIGURE 9 Effects of B/t ratios on $P-\varepsilon$ relationships.

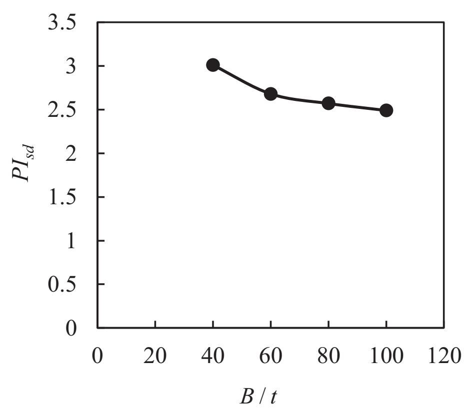

FIGURE 10 Effects of B/t ratios on ductility of steel-reinforced concrete-filled steel tubular columns.

underestimation of the ultimate strength of the short SRCFST column by 26.2%. This means that the concrete confinement has a significant contribution to the load-carrying capacity of short SRCFST columns; therefore, it must be considered in the inelastic analysis and design of such filled composite columns. As shown in Figure 16, the concrete confinement has minor effect on the initial stiffness of the SRCFST column and considerable effect on the postpeak behavior and residual strength of the column.

6 | RELATIVE SIGNIFICANCE OF PARAMETERS

A sensitivity analysis was conducted to determine the relative significance of the parameters on the strength of SRCFST columns. A correlation matrix is a useful tool in this process as it can reveal which variable has the strongest correlation with the output. This statistical tool can provide valuable insights into the relations between various parameters and their impact on responses, as demonstrated by Abdel Aleem et al.[26] Figure 17 depicts the correlation plot for the parameters considered in this study. The correlation values range from −1.0 to 1.0, where a value of 1.0 represents a perfectly direct relationship, a zero value denotes no correlation, and $a - 1$ value indicates a perfect inverse relationship between the pairs of parameters under investigation. It appears that the B/t ratio and the steel ratio are negatively correlated, implying that these two parameters are interdependent.

The analysis indicates a very strong correlation between the ultimate axial load and concrete strength,

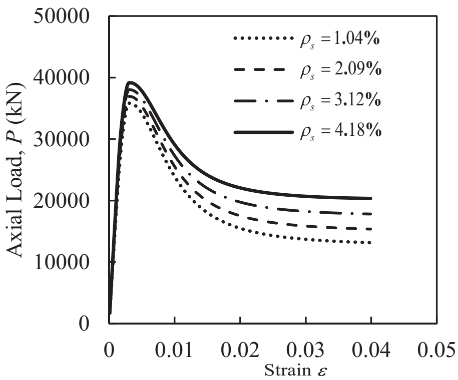

FIGURE 11 Effects of ρ_s ratio on $P-\varepsilon$ relationships.

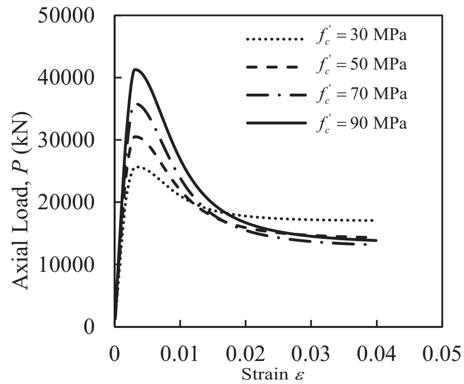

FIGURE 13 Influences of concrete strengths on $P-\varepsilon$ relationships.

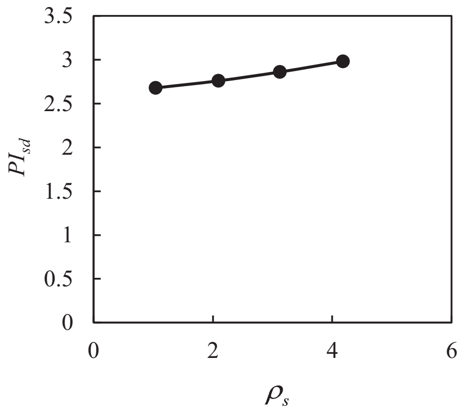

FIGURE 12 Effects of ρ_s ratio on ductility.

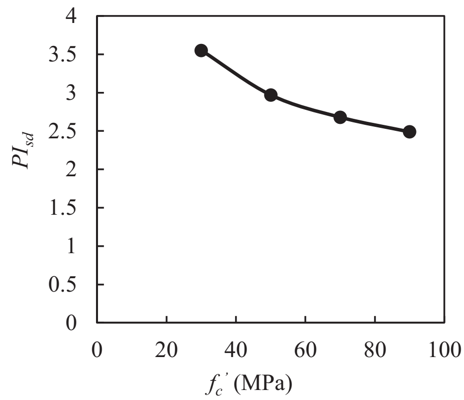

FIGURE 14 Effects of concrete strengths on ductility.

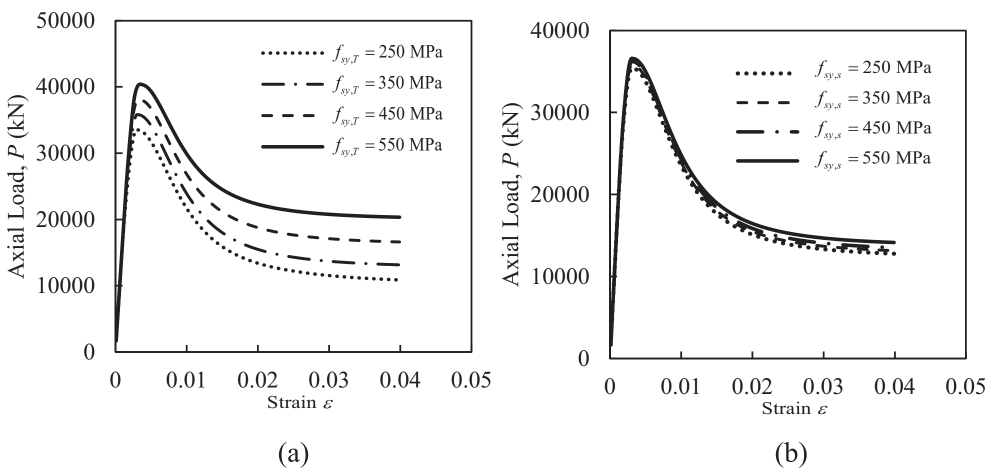

FIGURE 15 The impacts of steel yield stresses of (a) steel tube and (b) internal steel profile on the $P-\varepsilon$ curves of SRCFST columns.

which suggests that the concrete strength is a critical property in estimating the axial capacity of SRCFST columns. The axial capacity is moderately correlated with the outer tube's steel ratio and yield strength. However, the ultimate axial load is almost uncorrelated with the yield stress of the embedded steel section. This is consistent with the findings discussed in preceding sections. Moreover, the width-to-thickness ratio negatively correlates with the ultimate axial load, as the outer tube may experience local buckling for a high ratio.

The order of the relative significance of the parameters on the ultimate axial load of SRCFST columns is as follows: (1) concrete strengths f'_c, (2) steel ratio ρ_s, (3) yield stress of the outer tube $f_{sy,T}$, (4) width-to-thickness ratio (B/t), and (5) yield stress of the embedded section $f_{sy,s}$.

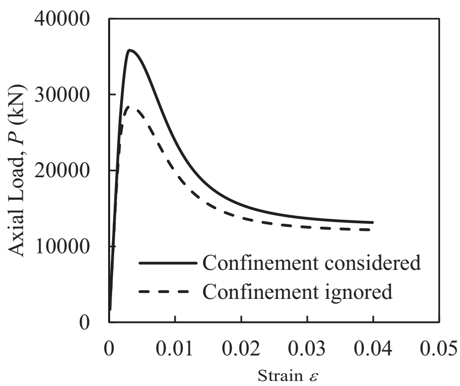

FIGURE 16 Confinement effect on the load-strain responses of steel-reinforced concrete-filled steel tubular columns.

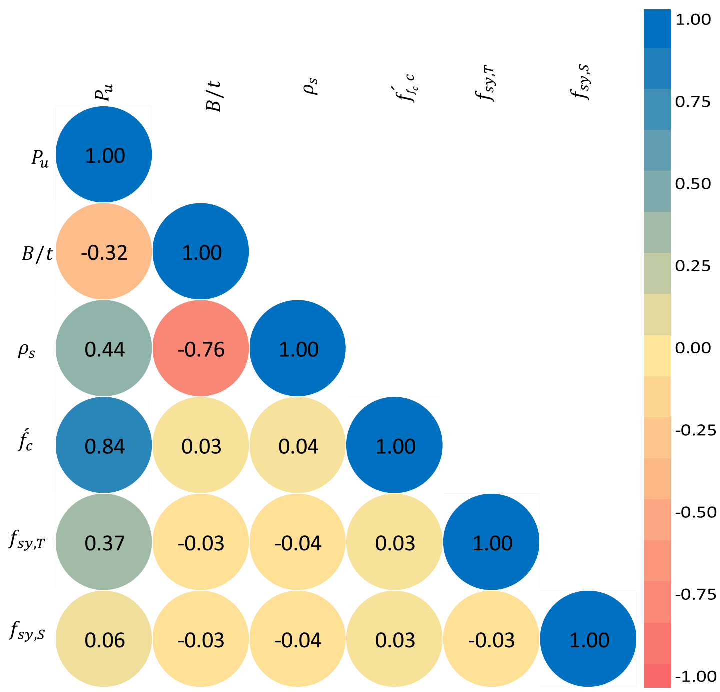

FIGURE 17 Correlation matrix of input parameters.

7 | DESIGN MODELS

7.1 | Current design codes

In this section, the effectiveness of current standards, including AISC 360–16,[27] Eurocode 4,[28] ACI 318–11,[29] and DBJ 13–51-2010[30] in estimating the ultimate strength of axially loaded SRCFST columns is investigated. Table 5 presents the formulas specified in these standards for determining the ultimate axial strength of SRCFST columns. The accuracy of the design formulas is evaluated by comparisons of calculations with experimental data given in Table 1 and the numerical solutions of columns listed in Table 4. It can be seen from Table 6 that the current design codes specified for square CFST columns are inadequate in predicting the ultimate strengths of SRCFST columns. All design standards significantly underestimate the ultimate loads of SRCFST columns. Therefore, there is a need for developing an accurate design formula for SRCFST columns under axial compression.

7.2 | Proposed design formula

A design equation for estimating the ultimate strength of SRCFST columns is proposed herein as

$$P_{u,des} = A_{st} f_{sy,T} + A_{ss} f_{sy,S} + \left(\gamma_c f'_c + 4.1 f_{rp}\right) A_c \quad (17)$$

in which f_{rp} is calculated using Equation (13).

TABLE 5 Design expressions for steel-reinforced concrete-filled steel tubular columns using the standards of concrete-filled steel tubular columns.

Standard	Design equations	Design limitations
AISC 360–16[27]	$P_{\mathrm{u,AISC}} = \begin{cases} P_o\left[0.658^{(P_o/P_e)}\right] & \text{for } P_e \geq 0.44P_o \\ 0.877P_e & \text{for } P_e < 0.44P_o \end{cases}$ $P_o = A_{\mathrm{st}}f_{\mathrm{sy,T}} + A_{\mathrm{ss}}f_{\mathrm{sy,S}} + C_2A_cf_c^{'}$ $P_{\mathrm{e}} = \frac{\pi^2}{(\mathrm{KL})^2}(\mathrm{EI})_{\mathrm{eff}}$ $(\mathrm{EI})_{\mathrm{eff}} = E_{\mathrm{st}}I_{\mathrm{st}} + E_{\mathrm{ss}}I_{\mathrm{ss}} + C_4E_cI_c$ $C_4 = 0.6 + 2\left(\frac{A_{\mathrm{st}}+A_{\mathrm{ss}}}{A_{\mathrm{st}}+A_{\mathrm{ss}}+A_c}\right) \leq 0.9$ where $C_2 = 0.85$	$B/t \leq 2.26\sqrt{E_s/f_{\mathrm{sy}}}$ $21 \leq f_c^{'} \leq 70\,\mathrm{MPa}$
Eurocode 4[28]	$P_{\mathrm{u,EC4}} = A_{\mathrm{st}}f_{\mathrm{sy},T} + A_{\mathrm{ss}}f_{\mathrm{sy},S} + A_cf_c^{'}$	$B/t \leq 52\sqrt{235/f_{\mathrm{sy}}}$ $235 \leq f_{\mathrm{sy}} \leq 460\,\mathrm{MPa}$ $20 \leq f_c^{'} \leq 60\,\mathrm{MPa}$
DBJ 13–51-2010[30]	$P_{\mathrm{u,DBJ}} = f_{\mathrm{sc}}(A_{\mathrm{st}} + A_{\mathrm{ss}} + A_{\mathrm{c}})$ $f_{\mathrm{sc}} = f_{\mathrm{ck}}(1.18 + 0.85\xi)$ $f_{\mathrm{ck}} = 0.67f_{\mathrm{cu}}$	$B/t \leq 60\sqrt{235/f_{\mathrm{sy}}}$ $235 \leq f_{\mathrm{sy}} \leq 420\,\mathrm{MPa}$ $24 \leq f_c^{'} \leq 70\,\mathrm{MPa}$
ACI 318–11[29]	$P_{\mathrm{u,ACI}} = A_{\mathrm{st}}f_{\mathrm{sy,T}} + A_{\mathrm{ss}}f_{\mathrm{sy,S}} + 0.85A_cf_c^{'}$	$B/t \leq \sqrt{3E_s/f_{\mathrm{sy}}}$ $f_c^{'} \geq 17.2\,\mathrm{MPa}$

TABLE 6 Evaluating the accuracy of design codes in predicting the maximum strengths of steel-reinforced concrete-filled steel tubular (SRCFST) short columns.

		AISC 360–16		Eurocode 4		DBJ 13-51-2010		ACI 318–11		Proposed in this study	
Specimen	$P_{\mathrm{u,exp}}$ (kN)	$P_{\mathrm{u,AISC}}$ (kN)	$\frac{P_{\mathrm{u,AISC}}}{P_{\mathrm{u,exp}}}$	$P_{\mathrm{u,EC4}}$ (kN)	$\frac{P_{\mathrm{u,EC4}}}{P_{\mathrm{u,exp}}}$	$P_{\mathrm{u,DBJ}}$ (kN)	$\frac{P_{\mathrm{u,DBJ}}}{P_{\mathrm{u,exp}}}$	$P_{\mathrm{u,ACI}}$ (kN)	$\frac{P_{\mathrm{u,ACI}}}{P_{\mathrm{u,exp}}}$	$P_{\mathrm{u,prop}}$ (kN)	$\frac{P_{\mathrm{u,prop}}}{P_{\mathrm{u,exp}}}$
S5L10V	4035	3226	0.80	3443	0.85	3743	0.93	3252	0.81	4097	1.02
S5L10	4050	3226	0.80	3443	0.85	3743	0.92	3252	0.80	4097	1.01
S5H10V	4880	3723	0.76	4035	0.83	4396	0.90	3755	0.77	4543	0.93
S5H10	4880	3723	0.76	4035	0.83	4396	0.90	3755	0.77	4543	0.93
S4L10	3930	3043	0.77	3264	0.83	3471	0.88	3068	0.78	3912	1.00
S4H10	4750	3552	0.75	3870	0.81	4124	0.87	3583	0.75	4379	0.92
S4L10I	3410	2611	0.77	2838	0.83	2893	0.85	2634	0.77	3442	1.01
S4H14	4710	3799	0.81	4106	0.87	4514	0.96	3829	0.81	4629	0.98
S5L10I	3620	2794	0.77	3018	0.83	3141	0.87	2818	0.78	3627	1.00
PY10I-0-3	3740	3050	0.82	3293	0.88	3372	0.90	3079	0.82	3930	1.05
STSRC235-3-H	3729	3252	0.87	3678	0.99	3677	0.99	3292	0.88	3964	1.06
STSRC235-4-H	4239	3426	0.81	3842	0.91	3929	0.93	3465	0.82	4156	0.98
STSRC235-5-H	4545	3598	0.79	4005	0.88	4189	0.92	3637	0.80	4316	0.95
STSRC345-3-H	4114	3444	0.84	3875	0.94	3871	0.94	3489	0.85	4130	1.00
STSRC345-4-H	4231	3682	0.87	4104	0.97	4191	0.99	3727	0.88	4396	1.04
STSRC235-2-DH	4153	3382	0.81	3793	0.91	3886	0.94	3416	0.82	4046	0.97

(Continues)

TABLE 6 (Continued)

Specimen	$P_{u,exp}$ (kN)	AISC 360–16 $P_{u,AISC}$ (kN)	$\frac{P_{u,AISC}}{P_{u,exp}}$	Eurocode 4 $P_{u,EC4}$ (kN)	$\frac{P_{u,EC4}}{P_{u,exp}}$	DBJ 13-51-2010 $P_{u,DBJ}$ (kN)	$\frac{P_{u,DBJ}}{P_{u,exp}}$	ACI 318–11 $P_{u,ACI}$ (kN)	$\frac{P_{u,ACI}}{P_{u,exp}}$	Proposed in this study $P_{u,prop}$ (kN)	$\frac{P_{u,prop}}{P_{u,exp}}$
STSRC235-3-DH	4553	3557	0.78	3959	0.87	4153	0.91	3592	0.79	4253	0.93
STSRC235-4-DH	4577	3730	0.81	4124	0.90	4429	0.97	3765	0.82	4445	0.97
STSRC235-3DH*	4223	3262	0.77	3685	0.87	3689	0.87	3299	0.78	3971	0.94
SRCSFT 1	39,293	32,360	0.82	36,080	0.92	37,065	0.94	32,708	0.83	38,619	0.98
SRCSFT 2	35,833	29,025	0.81	32,860	0.92	32,446	0.91	29,367	0.82	34,955	0.98
SRCSFT 3	33,888	27,330	0.81	31,229	0.92	30,226	0.89	27,675	0.82	32,859	0.97
SRCSFT 4	32,542	26,304	0.81	30,244	0.93	28,922	0.89	26,653	0.82	31,855	0.98
SRCSFT 5	35,833	29,025	0.81	32,860	0.92	32,446	0.91	29,367	0.82	34,955	0.98
SRCSFT 6	36,942	30,101	0.81	33,912	0.92	33,919	0.92	30,459	0.82	36,088	0.98
SRCSFT 7	38,040	31,172	0.82	34,952	0.92	35,410	0.93	31,538	0.83	37,209	0.98
SRCSFT 8	39,170	32,287	0.82	36,024	0.92	36,981	0.94	32,650	0.83	38,363	0.98
SRCSFT 9	25,645	17,900	0.70	19,554	0.76	19,506	0.76	18,057	0.70	24,773	0.97
SRCSFT 10	30,518	23,469	0.77	26,207	0.86	25,976	0.85	23,712	0.78	29,638	0.97
SRCSFT 11	35,833	29,025	0.81	32,860	0.92	32,446	0.91	29,367	0.82	34,955	0.98
SRCSFT 12	41,301	34,566	0.84	39,513	0.96	38,916	0.94	35,022	0.85	40,422	0.98
SRCSFT 13	33,516	26,717	0.80	30,500	0.91	30,030	0.90	27,007	0.81	32,912	0.98
SRCSFT 14	35,833	29,025	0.81	32,860	0.92	32,446	0.91	29,367	0.82	34,955	0.98
SRCSFT 15	38,123	31,327	0.82	35,220	0.92	34,862	0.91	31,727	0.83	36,997	0.97
SRCSFT 16	40,410	33,626	0.83	37,580	0.93	37,278	0.92	34,087	0.84	39,040	0.97
SRCSFT 17	35,433	28,658	0.81	32,484	0.92	32,061	0.90	28,992	0.82	34,546	0.97
SRCSFT 18	35,833	29,025	0.81	32,860	0.92	32,446	0.91	29,367	0.82	34,955	0.98
SRCSFT 19	36,227	29,391	0.81	33,236	0.92	32,831	0.91	29,743	0.82	35,364	0.98
SRCSFT 20	36,611	29,758	0.81	33,611	0.92	33,215	0.91	30,119	0.82	35,773	0.98
Mean			0.80		0.89		0.91		0.81		0.98
Standard deviation			0.03		0.05		0.04		0.03		0.03
Coefficients of variance			0.04		0.05		0.04		0.04		0.03

To assess the accuracy of the proposed equation, the ultimate strengths of the SRCFST columns calculated by using Equation (17) are compared with test results in Table 6. It would appear that the proposed equation yields accurate strength predictions of SRCFST columns, providing a mean predicting-to-experimental strength ratio of 0.98 and a standard deviation of 0.03.

8 | CONCLUSIONS

This paper has presented a numerical model developed for computational simulation of the inelastic responses of axially loaded SRCFST columns recognizing the localized buckling of the external square steel box. The proposed inelastic simulation model considering concrete confinement accurately predicts the responses of SRCFST columns. The behavior of SRCFST columns is found to be affected by several parameters, including the ratio of width-to-thickness (B/t), steel ratio (ρ_s), concrete strength, and yield strength of the steel sections. The suggested simplified design formula is demonstrated to give more accurate strength calculations of SRCFST short columns than existing design codes. Therefore, the study provides valuable insights into the nonlinear analysis, behavior, and design of SRCFST columns under axial loading. The proposed confinement model can be implemented in numerical analysis procedures for simulating the responses of SRCFST columns.

NOMENCLATURE

A_c	cross-sectional area of concrete
$A_{c,j}$	concrete element area of fiber j
$A_{s,i}$	steel element area of fiber i
A_{ss}	cross-sectional area of embedded steel section
A_{st}	cross-sectional area of external steel tube
B	width of the outer tube
D_c	effective diameter $=(B-2t)$
E	elasticity modulus
$f_c^{'}$	unconfined concrete cylindrical strength
$f_{cc}^{'}$	concrete compressive strength
f_{rp}	lateral pressure to the core concrete
f_{su}	steel tensile strength
f_{sy}	steel yield strength
$f_{sy,T}$	yield stress of the outer steel tube
$f_{sy,S}$	yield stress of the embedded steel section
nc	total concrete elements
ns	total steel elements
P	axial load
$P_{u,exp}$	test ultimate strength
$P_{u,num}$	ultimate strength obtained using fiber analysis
$P_{u,FE}$	ultimate strength obtained using finite element analysis
t	thickness of the outer tube
γ_c	reduction of concrete strength due to the columns size effect $\gamma_c = 1.85 D_c^{-0.135}$
$\varepsilon_{0.90}$	axial compressive strain at which the column's axial load reduces to 90% of its maximum load
$\varepsilon_{0.75}$	Axial compressive strain at which the column's axial load reaches 75% of its maximum load
ε_c	concrete strain
$\varepsilon_{cc}^{'}$	concrete compressive strain
ε_s	strain of the steel fibers
ε_{st}	hardening strain $= 0.005$
ε_{su}	steel tensile strain
ε_{sy}	steel yield strain
ε_y	yield strain determined as $\varepsilon_{0.75}/0.75$
σ_c	concrete stress
$\sigma_{s,i}$	longitudinal steel stress of element i
$\sigma_{c,j}$	longitudinal concrete of element j
σ_s	stress of the steel fibers

ACKNOWLEDGMENT

Open access publishing facilitated by Victoria University, as part of the Wiley - Victoria University agreement via the Council of Australian University Librarians.

DATA AVAILABILITY STATEMENT

The data that support the findings of this study are available from the corresponding author upon reasonable request.

ORCID

Mohamed Emara https://orcid.org/0000-0003-4936-5257
Qing Quan Liang https://orcid.org/0000-0003-0333-2265

REFERENCES

1. Lai B-L, Zhang M-Y, Zheng X-F, Chen Z-P, Zheng Y-Y. Experimental study on the axial compressive behaviour of steel reinforced concrete composite columns with stay-in-place ECC jacket. J Build Eng. 2023;68:106174.
2. Lai B, Liew JR, Le Hoang A. Behavior of high strength concrete encased steel composite stub columns with C130 concrete and S690 steel. Eng Struct. 2019;200:109743.
3. Wang J, Wang X, Duan Y, Su Y, Yi X. The investigation on mechanical performances of high-strength steel reinforced concrete composite short columns under axial load. Materials. 2022;15(1):329.
4. Ding F-X, Zhang T, Liu X-M, Lu Z-H, Guo Q, Jiang G-S. Behavior of steel-reinforced concrete-filled square steel tubular stub columns under axial loading. Thin Walled Struct. 2017;119:737–48.
5. Sakino K, Nakahara H, Morino S, Nishiyama I. Behavior of centrally loaded concrete-filled steel-tube short columns. J Struct Eng. 2004;130(2):180–8.
6. Zhu M, Liu J, Wang Q, Feng X. Experimental research on square steel tubular columns filled with steel-reinforced self-consolidating high-strength concrete under axial load. Eng Struct. 2010;32(8):2278–86.
7. Wang L, Zhao T, Li H. Experimental research and theoretical analysis of square steel tube columns filled with steel-reinforced high-strength concrete subjected to eccentric loading. J Build Struct. 2010;31(7):64–71. (in Chinese).
8. Wang JZ, Sun ML, Sun ML, Jia JQ. Axial load behavior and strength of tube-confined steel-reinforced short columns with ultra-high-strength concrete. Adv Struct Eng. 2018;21(3):428–44.
9. Persson PO, Strang G. A simple mesh generator in MATLAB. SIAM Rev. 2004;46(2):329–45.
10. Park R. Evaluation of ductility of structures and structural assemblages from laboratory testing. Bull N Z Natl Soc Earthq Eng. 1989;22(3):155–66.
11. Tao Z, Han LH, Zhao XL. Behaviour of concrete-filled double skin (CHS inner and CHS outer) steel tubular stub columns and beam-columns. J Constr Steel Res. 2004;60(8):1129–58.
12. Liang QQ. Nonlinear analysis of circular double-skin concrete-filled steel tubular columns under axial compression. Eng Struct. 2017;131:639–50.
13. Lai ZC, Varma AH. Effective stress-strain relationships for analysis of noncompact and slender filled composite (CFT) members. Eng Struct. 2016;124:457–72.
14. Liang QQ. Performance-based analysis of concrete-filled steel tubular beam–columns, part I: theory and algorithms. J Constr Steel Res. 2009;65(2):363–72.
15. Mander JB. Seismic design of bridge piers. Christchurch, New Zealand: Department of Civil Engineering, University of Canterbury; 1983 PhD Thesis.

16. Liang QQ, Uy B, Liew JYR. Local buckling of steel plates in concrete-filled thin-walled steel tubular beam–columns. J Constr Steel Res. 2007;63(3):396–405.
17. Mander JB, Priestley MJN, Park R. Theoretical stress-strain model for confined concrete. J Struct Eng. 1988;114(8):1804–26.
18. Ahmed M, Liang QQ, Patel VI, Hadi MNS. Nonlinear analysis of rectangular concrete-filled double steel tubular short columns incorporating local buckling. Eng Struct. 2018;175:13–26.
19. Wang Z, Tao Z, Han LH, Uy B, Lam D, Kang WH. Strength, stiffness and ductility of concrete-filled steel columns under axial compression. Eng Struct. 2017;135:209–21.
20. Lim JC, Ozbakkaloglu T. Stress–strain model for normal-and light-weight concretes under uniaxial and triaxial compression. Construct Build Mater. 2014;71:492–509.
21. Xiong MX, Xiong DX, Liew JYR. Axial performance of short concrete filled steel tubes with high-and ultra-high-strength materials. Eng Struct. 2017;136:494–510.
22. Oehlers DJ, Bradford MA. Elementary behaviour of composite steel and concrete structural members. Oxford UK: Butterworth-Heinemann; 1999.
23. Hu HT, Huang CS, Wu MH, Wu YM. Nonlinear analysis of axially loaded concrete-filled tube columns with confinement effect. J Struct Eng. 2003;129(10):1322–9.
24. Thai HT, Uy B, Khan M, Tao Z, Mashiri F. Numerical modelling of concrete-filled steel box columns incorporating high strength materials. J Constr Steel Res. 2014;102:256–65.
25. Tao Z, Katwal U, Uy B, Wang W-D. Simplified nonlinear simulation of rectangular concrete-filled steel tubular columns. J Struct Eng. 2021;147(6):04021061.
26. Abdel Aleem BH, Ismail MK, Haggag M, El-Dakhakhni W, Hassan AA. Interpretable soft computing predictions of elastic shear buckling in tapered steel plate girders. Thin Walled Struct. 2022;176:109313.
27. AISC. Specification for structural steel buildings. Chicago (IL), USA: American Institute of Steel Construction; 2016.
28. European Committee for Standardization (CEN). Eurocode 4: Design of composite steel and concrete structures-part 1–1: general rules and rules for buildings. Brussels, Belgium: European Committee for Standardization (CEN); 2004.
29. ACI 318–19. Building code requirements for structural concrete and commentary. Farmington Hills, Michigan, USA: ACI; 2019.
30. DBJ/13-51-2010. Technical specifications for concrete-filled steel tubular structures. Fuzhou, China: The Housing and Urban–Rural Development Department of Fujian Province; 2010.

AUTHOR BIOGRAPHIES

Mizan Ahmed, Centre for Infrastructure Monitoring and Protection, School of Civil and Mechanical Engineering, Curtin University, Kent Street, Bentley, WA 6102, Australia. Email: mizan.ahmed@curtin.edu.au.

Ramy I. Shahin, Department of Civil Engineering, Higher Institute of Engineering and Technology, Kafrelsheikh, Egypt. Email: ramy.shahin@kfs-hiet.edu.eg.

Saad A. Yehia, Department of Civil Engineering, Higher Institute of Engineering and Technology, Kafrelsheikh, Egypt. Email: saadyhy81@gmail.com.

Mohamed Emara, Structural Engineering Department, Faculty of Engineering, Zagazig University, Zagazig, 44,519, Egypt. Email: mohamed.r.emara@gmail.com.

Vipulkumar Ishvarbhai Patel, School of Computing, Engineering and Mathematical Sciences, La Trobe University, Bendigo, VIC 3552, Australia. Email: v.patel@latrobe.edu.au.

Qing Quan Liang, College of Sport, Health, and Engineering, Victoria University, PO Box 14,428, Melbourne, VIC 8001, Australia. Email: qing.liang@vu.edu.au.

How to cite this article: Ahmed M, Shahin RI, Yehia SA, Emara M, Patel VI, Liang QQ. Nonlinear analysis of square steel-reinforced concrete-filled steel tubular short columns considering local buckling. Structural Concrete. 2023. https://doi.org/10.1002/suco.202300402